MICROCOPY RESOLUTION TEST CHART

NATIONAL BUREAU OF STANDARDS 1963 A

AFOSR·TR· 8 6 - 2 0 0 4

1

②

FLUID DYNAMIC - STRUCTURAL

INTERACTIONS OF LABYRINTH SEALS

.anuel Martinez-Sanchez

John Dugundji

Gas Turbine and Plasma Dynamics Laboratory

Department of Aeronautics and Astronautics

Massachusetts Institute of Technology

Cambridge, Massachusetts 02139

May 1986

REPORT DOCUMENTATION PAGE

1a. REPORT SECURITY CLASSIFICATION	1b. RESTRICTIVE MARKINGS
2a. SECURITY CLASSIFICATION AUTHORITY	**3. DISTRIBUTION/AVAILABILITY OF REPORT** Approved for public release, distribution unlimited
2b. DECLASSIFICATION/DOWNGRADING SCHEDULE	

4. PERFORMING ORGANIZATION REPORT NUMBER(S)	5. MONITORING ORGANIZATION REPORT NUMBER(S) **AFOSR-TR- 86-2004**

6a. NAME OF PERFORMING ORGANIZATION Gas Turbine and Plasma Dynamics Laboratory, MIT	6b. OFFICE SYMBOL (If applicable)	7a. NAME OF MONITORING ORGANIZATION _Same as 8a_
6c. ADDRESS (City, State and ZIP Code) MIT, 77 Massachusetts Avenue 37-401 Cambridge, MA 02139		**7b. ADDRESS (City, State and ZIP Code)** _Same as 8c_
8a. NAME OF FUNDING/SPONSORING ORGANIZATION AFOSR	**8b. OFFICE SYMBOL (If applicable)** NA	**9. PROCUREMENT INSTRUMENT IDENTIFICATION NUMBER** AFOSR 83-0034

8c. ADDRESS (City, State and ZIP Code) Bolling Air Force Base Washington, DC 20332 - 6448	10. SOURCE OF FUNDING NOS.			
	PROGRAM ELEMENT NO.	PROJECT NO.	TASK NO.	WORK UNIT NO.
	61102F	2302	B1	

11. TITLE (Include Security Classification) Fluid Dynamic-Structural- Interactions of Labyrinth Seals

12. PERSONAL AUTHOR(S) M. Martinez-Sanchez and J. Dugundji

13a. TYPE OF REPORT Annual	13b. TIME COVERED FROM 12/1/82 TO 11/30/83	14. DATE OF REPORT (Yr., Mo., Day) June 3, 1986	15 PAGE COUNT 31

16. SUPPLEMENTARY NOTATION

17. COSATI CODES			18. SUBJECT TERMS (Continue on reverse if necessary and identify by block number)
FIELD	GROUP	SUB. GR.	

19. ABSTRACT (Continue on reverse if necessary and identify by block number)

An analytical model was formulated for the calculation of unsymmetrical pressure distributions inside the cavities of a multi-stage labyrinth seal. The model is based on a set of linearized continuity and momentum equations for the throughflow, and can account for the effects of rotation, whirl, flow swirl, differential gap width and (limited) compressibility. Preliminary calculations show excellent agreement with non-whirling side-force data in the literature. Also, models are being constructed that will permit calculation of the effect of these seal forces on the running stability of flexible, highly loaded turbomachines, with the Space Shuttle Main Engine serving as the prototype of such machines.

20. DISTRIBUTION/AVAILABILITY OF ABSTRACT UNCLASSIFIED/UNLIMITED ☐ SAME AS RPT ☐ DTIC USERS ☐	21 ABSTRACT SECURITY CLASSIFICATION
22a. NAME OF RESPONSIBLE INDIVIDUAL Anthony K Amos	**22b TELEPHONE NUMBER (Include Area Code)** 202 767-4937	**22c OFFICE SYMBOL** NA

DD FORM 1473, 83 APR EDITION OF 1 JAN 73 IS OBSOLETE Unclassified

ABSTRACT

An analytical model was formulated for the calculation of unsymmetrical pressure distributions inside the cavities of a multi-stage labyrinth seal. The model is based on a set of linearized continuity and momentum equations for the throughflow, and can account for the effects of rotation, whirl, flow swirl, differential gap width and (limited) compressibility. Preliminary calculations show excellent agreement with non-whirling side-force data in the literature. Also, models are being constructed that will permit calculation of the effect of these seal forces on the running stability of flexible, highly loaded turbomachines, with the Space Shuttle Main Engine serving as the prototype of such machines.

FORWARD

This report describes work done at the Gas Turbine and Plasma Dynamics Laboratory (GT&PDL) at the Massachusetts Institute of Technology for the Air Force under Grant No. AFOSR-83-0034. Dr. Anthony K. Amos was the technical monitor.

The work reported herein was performed during the period 1 December 1982 through 30 November 1983. Two graduate students, Otto W.K. Lee and Ya-Pei Chang, worked under the supervision of Professors Manuel Martinez-Sanchez and John Dugundji during this time.

1. INTRODUCTION

The purpose of this program was to investigate the fluid dynamic-structural interaction of labyrinth seals. This research is in an area of limiting technology in modern gas turbine engines. A better understanding of labyrinth seals and their improved design would reduce stage and secondary flow leakages, and thus lead to increased engine efficiency and performance. This improvement should be accomplished without compromising the rotor dynamic stability, which is known to be sensitive to the fluid dynamic forces arising at the seals (see References (1) and (2)).

The present investigation was divided into two main efforts, one involving a fluid dynamics investigation of the seal forces developed in a rotating labyrinth seal, and another involving the rotordynamic and structural dynamic stability of a rotating shaft system in the presence of labyrinth seals and conventional bearings. The investigation was envisaged as extending over more than one year.

WORK PERFORMED

(a) Fluid Dynamics of Seals

The literature for fluid dynamic modeling of labyrinth seals was reviewed. Recent efforts at comprehensive modeling of labyrinth seals have been made by Kostyuk[3],[4] and Iwatsubo[5]. These models considered multicavity seals with the shaft executing orbiting motion without [5], or with simultaneous canting[3],[4]. Both axial and rotational fluid motion was considered in the glands, although quite

simplified equations were used to describe the flow in each cavity and past each tooth. Numerical techniques were then resorted to in order to obtain overall forces from the original partial differential equations in time and azimuthal angle.

In parallel with these analytical attacks, detailed pressure measurements inside oscillating multicavity seals have also become recently available (Ref. 6). These data address a wide range of variables of interest, including relative rotational/whirl speeds, amplitudes, pre-swirl, number of cavities per seal, etc. They generated both pressure distributions in the glands and integrated spring and damping coefficients, for both colinear and quadrature forces.

The methods of Refs (3) to (5) held promise of providing a comprehensive and practical model capable of quantitative predictions at the design stage. Accordingly, a model of fluid forces in a labyrinth seal was fashioned after that of Iwatsubo[5]. Basically, it consisted of a momentum and a continuity equation for each of a number of seal glands executing small elliptic satellite oscillations. The inter-cavity flows were calculated using constant discharge coefficients and accounting for compressibility effects; the flow azimuthal velocity was calculated from a balance between friction on the fixed and movable parts of the seal, using conventional turbulent friction coefficients. After linearization for small perturbations, there resulted a set of linear, periodic coefficient equations for perturbation pressures, velocities, etc., in each of the glands of the

seal. To the first approximation, harmonic balance was used to reduce this to a system of partial differential equations in time and azimuth, with constant coefficients. The direct and quadrature components of each variable were then conveniently isolated, and by restricting attention to the quasi-steady state forced state (growth or decay time much longer than a period), the solution reduced to that of an algebraic set of equations in the respective direct and quadrature amplitudes and phase angles of all the variables. Integration around the seal then related these amplitudes to the desired force coefficients.

The method described above is a marked improvement over those used in Ref. (5) for example, where finite difference approximations were used to solve the governing equations. It is anticipated that this will permit introduction of refinements to the model while still remaining computationally economical.

The above labyrinth seal formulation is being written up as a Master's thesis by one of the two graduate students, and will become available in February 1984, Ref. 7. Also, a paper based on this formulation will be presented at the forthcoming 3rd Workshop on Rotor Dynamic Instability Problems in High Performance Turbomachinery (Texas A&M, May 28-30, 1984). A copy of this paper, giving the mathematical formulation of the labyrinth seals model, is included here as Appendix A of this report. Also, the Master's Thesis by A. Celorio (Ref. 9) was instrumental in initiating our seal modeling effort.

(b) Rotordynamic and Structural Dynamic Stability

Some basic literature for the dynamic stability of rotor systems was reviewed (Ref 10-14) together with some more recent work related to the space shuttle fuel turbopump (Refs. 15, 16). Using the traditional linear methods of rotor analysis, a simple model of the high pressure fuel turbopump (HPFTP) for the space shuttle is being set up based on the structural dynamic data given by Muller in Ref. 16. Equations of motion have been written for the rotating shaft assembly on the flexible supporting case structure, including provisions for labyrinth seal forces. The labyrinth seal forces, as determined from the fluid dynamic part of the investigation, generally involve frequency dependent stiffness and damping terms. These seal forces are being fitted here by means of Pade approximations to give frequency independent (constant coefficient) stiffness damping, mass and lag terms to be used in a traditional eigenvalue analysis to examine possible rotor instabilities. This is similar to procedures used in representing aerodynamic forces in aeroelastic analysis of aircraft (Ref. 17).

The above rotordynamic formulation is currently being pursued by the other of the two graduate students, and will become available as a Master's Thesis during the summer of 1984.

ACCOMPLISHMENTS

1. Formulation fluid Mechanics

2. Formulation Rotor dynamics will be continued next year.

REFERENCES

1.   Stoker, H.L., "Determining and Improving Labyrinth Seal Performance in Current and Advanced High Performance Gas Turbines," in Seal Technology in Gas Turbines, AGARD Conf. Proc. No. 237, 1978.

2.   Alford, J.S., "Protecting Turbomachinery from Self-Excited Rotor Whirl." Jnl. of Engineering for Power, Oct. 1965, pp. 333-344.

3.   Kostyuk, A.G., "A Theoretical Analysis of the Aerodynamic Forces in the Labyrinth Glands of Turbomachines". Teploenergetika , 19, (1), 1972, pp. 29-33.

4.   Kostyuk, A.G., Shatokin, V.F. and Ivanow, N.M., "Calculation of the Threshold Capacity of Large Turbine-Generators," Teploenergetika, 21, (3), 1974, pp. 19-25.

5.   Iwatsubo, T., "Evaluation of Instability Forces of Labyrinth Seals in Turbines and Compressors." In Rotordynamic Instability Problems in High Performance Turbomachinery. NASA Conf. Publ. 2133, pp. 139-168 (1980).

6.   Benchkert, H., and Wachter, J., "Flow-Induced Spring Coefficients of Labyrinth Seals for Application in Rotor Dynamics." In Rotordynamic Instability Problems in High-Performance Turbomachinery. NASA Conf., Publ. 2133, 1980, pp. 189-212.

7.   Lee, O.W.K., "Prediction of Aerodynamic Force Coefficients in Labyrinth Seals", MIT, Department of Aeronautics and Astronautics, S.M. Thesis. February 1984.

8.   Lee., O.W.K., Martinez-Sanchez, M. and Czajkowski, E., "The Prediction of Force Coefficients for Labyrinth Seals." Proceedings of the III Workshop on Rotor Dynamic Instability Problems in High Performance Turbomachinery, Texas A&M University, May 28-30, 1984.

9.   Celorio-Villasenor, A., "Analysis of Distrubing Aerodynamic Forces in Labyrinth Seals". S.M. Thesis, Dept of Aeronautics and Astronautics, MIT, Sep. 1982.

10.   Smith, D.M., "The Motion of a Rotor Carried by a Flexible Shaft in Flexible Bearings." Proc. Royal Soc., (A) 142, 1933, pp 92-118.

11.   Dimentberg, F.M., Flexural Vibrations of Rotating Shafts, Butterworths, London, 1961.

12.   Tondl, A., _Some Problems of Rotor Dynamics_, Chapman and Hall, London, 1965.

13.   Gunter, E.J., Jr., "Dynamic Stability of Rotor-Bearing Systems." NASA SP-113, 1966.

14.   Childs, D.W., "The Space Shuttle Main engine High Pressure Fuel Turbopump Rotordynamic Instability Problem," Journal of Applied Mechanics, Vol. 100, January 1978, pp 48-57.

15.   Ek, M.C., "Solution of the Subsynchronous Whirl Problem in the High Pressure Hydrogen Turbomachinery of the Space Shuttle Main Engine," Proceedings of the 14th AIAA/SAE Joing Propulsion Conference, Las Vegas, Nevada, July 25-27, 1978, AIAA Paper 78-1002.

16.   Muller, G.R., "Finite Element Models of the Space Shuttle Main Engine," NASA TM-78260, NASA Marshall Space Flight Center, Alabama, January 1980.

17.   Edwards, J.W., Ashley, H., and Breakwell, J.V., "Unsteady Aerodynamic Modeling for Arbitrary Motions", AIAA J. Vol. 17, No. 4, April 1979, pp. 365-374.

APPENDIX A

Copy of paper to be presented at the 3rd Workshop on Rotordynamic Instability Problems in High Performance Turbomachinery, Texas A&M Univ. (28-30 May, 1984).

THE PREDICTION OF FORCE COEFFICIENTS FOR LABYRINTH SEALS

Otto W.K. Lee, M. Martinez-Sanchez and Eva Czajkowski
Massachusetts Institute of Technology
Cambridge, MA 02139, U.S.A.

1. Introduction

Fluid-dynamic forces arising from nonuniform pressure patterns in labyrinth seal glands are known to be potentially destabilizing in high power turbomachinery. A well documented case in point is that of the space Shuttle Main Engine turbopumps (ref. 1), and other examples can be found in the literature, as for instance in the recent review of Ehrich (ref. 2) and Childs and Ehrich (ref. 3). Seal forces are also an important factor for the stability of shrouded turbines, acting in that case in conjunction with the effects of blade-tip clearance variations (refs. 4,5).

The basic mechanisms which produce the uneven pressure distribution in a labyrinth have been qualitatively or semi-qualitatively discussed in many references (refs. 6,7). In most instances, the basic agent is found to be flow swirl in the glands, either from pre-swirl (as in the case of turbine shrouds) or from frictional interaction with the rotating shaft (as in multichamber jet engine seals). Quantitative modeling of these forces has also been reported by a number of authors (refs. 8, 9,10), using lumped-parameter models for each gland. These models yield in general predictions of the direct and cross-wise stiffnesses and damping coefficients for small shaft displacements, and are useful for linear stability analyses. Non-linear predictions for fully developed unstable operation are less advanced.

Fairly extensive data also exist on the stiffness factors of seals of various geo-metries (refs. 4,5,11,12,13). These have been generally obtained in rotary rigs with adjustable shaft eccentricity. Much less satisfactory is the situation with respect to data on damping coefficients due to labyrinth seals, since these require dynamic measurements on either vibrating shafts, or shafts fitted with adjustable whirl mech-anisms. Yet these data are almost as essential as those on stiffnesses, since the corresponding induced forces are of the same order. Ref.(13) reports damping data for non-rotating shafts.

In this paper we report on the development of a linear model for the prediction of labyrinth seal forces and on its comparison to available stiffness data. We also present a discussion of the relevance of fluid damping forces and report on the pre-liminary stages of a program to obtain data on these forces.

2. Model Formulation

The model is very similar in its main outline to those of Kostyuk (ref. 8) and Iwatsubo (ref. 9). It describes the flow of an ideal gas through the seal chambers, assuming largely constant temperature, but allowing for isentropic acceleration to-wards the narrow gaps and also for isentropic azimuthal flow redistribution in each chamber. Each chamber is assigned a pressure P_i and azimuthal velocity c_i, and these quantities are governed by equations of mass and azimuthal momentum conservation, written in integral form.

The axial flow rate q through each seal throttling is approximated by a commonly

used expression, which basically derives from Bernoulli's equation with a density halfway between those of the two adjacent chambers. Per unit length in the azimuthal direction, this gives

$$q_i = \mu_i \delta_i \sqrt{\frac{P_{i-1}^2 - P_i^2}{R_g T}} \tag{1}$$

where δ_i is the width of the narrow gap (see fig. 1) and $\mu_i = c_c \beta_i$ is the product of the usual contraction coefficient c_c times a carryover factor $\beta^c i$ to account for nonzero upstream axial velocity and nonzero pressure recovery in the downstream chamber. Eq. (1) is assumed to apply locally at each time t and azimuth ϕ. This semi-incompressible approximation is known to be reasonable up to gap Mach numbers of about 0.5; however, the last gap or two of a labyrinth with a high overall pressure ratio may be above that M ach number, and, in particular, the last chamber may choke. We have partially accommodated this effect by retaining Eq. (1) throughout, but replacing it by a choked-flow expression in the last chamber only if the first approximation indicates sonic or supersonic conditions there.

With reference to the geometry of fig. 1, the governing equations within each chamber are

$$\frac{\partial}{\partial t} (\rho_i f_i) + \frac{\partial}{\partial w} (\rho_i f_i c_i) + q_{i+1} - q_i = 0 \tag{2}$$

$$\frac{\partial}{\partial t} (\rho_i f_i c_i) + \frac{\partial}{\partial w} (\rho_i f_i c_i^2) + q_{i+1} c_i - q_i c_{i-1} + \tau_i' U' - \tau_i'' U'' + f_i \frac{\partial P_i}{\partial w} = 0 \tag{3}$$

These equations are first linearized about a condition of zero eccentricity. The zero'th order approximation provides a basic flow rate q^* and pressure and azimuthal velocity distributions P_i^*, c_i^*, (Appendix 1). The first approximation then provides linear equations for the perturbations, defined by

$$P_i = P_i^* (1 + \xi_i) \quad ; \quad q_i = q_i^* (1 + \zeta_i) \quad ; \quad c_i = c_i^* (1 + \eta_i) \tag{4}$$

where ξ_i, ζ_i, η_i are functions of t and $w = R_s \phi$. The right hand sides of these equations are determined by an assumed eccentric motion of the shaft, whose center follows an elliptic path

$$x_c = r_1 \cos \Omega t \quad ; \quad y_c = r_2 \sin \Omega t \tag{5}$$

where Ω is the shaft vibration frequency, closely identified with one of its natural frequencies.

The details of the analysis are given in references 14 and 15. For convenient solution, the perturbations (for a stationary oscillation) are expressed in the form

$$\xi = R_e [e^{i\Omega t}(\hat{\xi}_s \sin \phi + \hat{\xi}_c \cos \phi)] \ , \ \text{etc.} \tag{6}$$

where R_e indicates the real part, and $\hat{\xi}_s$, $\hat{\xi}_c$ are in general complex numbers. After elimination of ζ_i , the following system of perturbation equations is obtained:

$$
\begin{bmatrix}
-F_i & 0 & 0 & 0 \\
0 & -F_i & 0 & 0 \\
-Q_i & 0 & -S_i & 0 \\
0 & -Q_i & 0 & -S_i
\end{bmatrix}
\begin{Bmatrix}
\hat{\xi}_{s_{i-1}} \\
\hat{\xi}_{c_{i-1}} \\
\hat{\eta}_{s_{i-1}} \\
\hat{\eta}_{c_{i-1}}
\end{Bmatrix}
+
\begin{bmatrix}
E_i + i\Omega A_i & -B_i & 0 & -C_i \\
B_i & E_i + i\Omega A_i & C_i & 0 \\
P_i + i\Omega K_i & -M_i & R_i + i\Omega L_i & -N_i \\
M_i & P_i + i\Omega K_i & N_i & R_i + i\Omega L_i
\end{bmatrix}
\begin{Bmatrix}
\hat{\xi}_{s_i} \\
\hat{\xi}_{c_i} \\
\hat{\eta}_{s_i} \\
\hat{\eta}_{c_i}
\end{Bmatrix}
+
$$

$$
+
\begin{bmatrix}
-D_i & 0 & 0 & 0 \\
0 & -D_i & 0 & 0 \\
-0_i & 0 & 0 & 0 \\
0 & -0_i & 0 & 0
\end{bmatrix}
\begin{Bmatrix}
\hat{\xi}_{s_{i+1}} \\
\hat{\xi}_{c_{i+1}} \\
\hat{\eta}_{s_{i+1}} \\
\hat{\eta}_{c_{i+1}}
\end{Bmatrix}
=
\begin{Bmatrix}
-Z_i r_1 + \Omega J_i r_2 \\
i\Omega J_i r_1 - i Z_i r_2 \\
-Y_i r_1 + (-i W_i + \Omega X_i) r_2 \\
(W_i + i\Omega X_i) r_1 - i Y_i r_2
\end{Bmatrix}
\qquad (7)
$$

The expressions for the coefficients A_i , B_i , ... , Z_i are given in Appendix 2. For a seal with K chambers, i would range from $i = 1$ to K. The calculations reported here have assumed uniform inlet and exit conditions.

The forces are then obtained by integration of the perturbation pressures $P_i^* \xi_i(\phi)$ around the periphery of each chamber, followed by summation for all chambers. Since our attention will be restricted to the practical case of circular whirl ($r_1 = r_2 = r$), it is advantageous to project the forces in the directions towards the instantaneous minimum gap (F_d) and 90° ahead of it in the whirl direction (F_q), as shown in fig. 2. We obtain

$$
F_{d_i} = -R_s \ell_i \int_0^{2\pi} P_i^* \xi_i \cos(\phi - \Omega t) \, d\phi \qquad (8a)
$$

$$
F_{q_i} = -R_s \ell_i \int_0^{2\pi} P_i^* \xi_i \sin(\phi - \Omega t) \, d\phi \qquad (8b)
$$

These components can be expected to be time-invariant for a symmetric shaft in circular whirl. For this case, the form of the system of equations (7) indicates that we must have

$$
\hat{\xi}_{c_i} = i \hat{\xi}_{s_i} \quad ; \quad \hat{\eta}_{c_i} = i \hat{\eta}_{s_i} \qquad (9a,b)
$$

and the system (7) reduces to

$$
\begin{bmatrix} -F_i & 0 \\[2mm] -Q_i & -S_i \end{bmatrix}
\begin{Bmatrix} \hat{\xi}_{s_{i-1}} \\[2mm] \hat{\eta}_{s_{i-1}} \end{Bmatrix}
+
\begin{bmatrix} E_i + i\,(-B_i + \Omega A_i) & -iC_i \\[2mm] P_i + i\,(-M_i + \Omega K_i) & R_i + i(-N_i + \Omega L_i) \end{bmatrix}
\begin{Bmatrix} \hat{\xi}_{s_i} \\[2mm] \hat{\eta}_{s_i} \end{Bmatrix}
+
$$

$$
+
\begin{bmatrix} -D_i & 0 \\[2mm] -O_i & 0 \end{bmatrix}
\begin{Bmatrix} \hat{\xi}_{s_{i+1}} \\[2mm] \hat{\eta}_{s_{i+1}} \end{Bmatrix}
=
\begin{Bmatrix} -Z_i + \Omega J_i \\[2mm] -Y_i + \Omega X_i - iW_i \end{Bmatrix} r
\tag{10}
$$

Also, the complex force vector $F_{d_i} + i\,F_{q_i}$ is found to be given simply by

$$
F_{d_i} + i\,F_{q_i} = \pi\,R_s\,P_i^{*}\,(-i\,\hat{\xi}_{s_i})\,\ell_i
\tag{11}
$$

whereas, if the forces F_x and F_y along fixed directions Ox, Oy are desired, they are given by

$$
F_{x_i} + i\,F_{y_i} = (F_{d_i} + i\,F_{q_i})\,e^{i\Omega t}
\tag{12}
$$

3. The stiffness and damping coefficients

Most data reported to date on seal forces refer to situations with a static off-set, i.e., with $\Omega = 0$. Within a linear approximation, it is then unambiguous to define the direct and crosswise stiffness K_{xx}, K_{xy}, as $-F_d/r$ and $-F_q/r$, respectively. In practice, however, unstable whirl is observed to occur at or near (one of) the shaft natural frequencies, usually at the first one, Ω_o (and it first shows up at rotational frequencies ω of the order of twice this natural frequency). For purposes of dynamic modeling, then, it is of interest to calculate or measure the forces for $\Omega \simeq \Omega_o$, since the fluid disturbances are expected to translate into relatively small real and imaginary departures of Ω from its basic resonance value. A common expression for the disturbance forces in terms of the x_c, y_c deviations of the shaft center is

$$
\begin{cases}
F_x = -K_{xx}x_c + K_{xy}y_c - C_{xx}\dot{x}_c + C_{xy}\dot{y}_c \\[4mm]
F_y = -K_{xy}x_c - K_{xx}y_c - C_{xy}\dot{x}_c - C_{xx}\dot{y}_c
\end{cases}
\tag{13}
$$

where the stiffnesses K_{ij} and damping factors C_{ij} are taken to be constant. This amounts to an approximation in which terms proportional to $\ddot{x}_c$, $\bar{x}_c$, etc., are all neglected. It is easy to show that the corresponding approximation in terms of Ω is

one where the actual functions $F_d(\Omega)$, $F_q(\Omega)$ are replaced by their tangents at the frequency of interest:

$$\begin{cases} F_d(\Omega) \simeq F_{d_o} + F_{d_1}(\Omega - \Omega_o) \\[2mm] F_q(\Omega) \simeq F_{q_o} + F_{q_1}(\Omega - \Omega_o) \end{cases} \tag{14}$$

and then the K and C coefficients are given by

$$K_{xx} = -\frac{F_{d_o} - \Omega_o F_{d_1}}{r} \qquad C_{xx} = -\frac{F_{q_1}}{r}$$

$$\tag{15}$$

$$K_{xy} = -\frac{F_{q_o} - \Omega_o F_{q_1}}{r} \qquad C_{xy} = +\frac{F_{d_1}}{r}$$

Thus, determination (either analytical or experimental) of F_d, F_q at two whirling frequencies near Ω_o is sufficient to extract the K and C coefficients in this formulation.

An alternative formulation is often found in the literature (refs. 8,9,15) and is, in fact, the basis for the results presented here. Analytically, it consists of solving the system of equations (7) for $r_2 = 0$, i.e., for a <u>linear</u> vibratory shaft motion, and adscribing to $-K_{xx}x_c$, $K_{xy}x_c$ those forces F_d, F_q in time phase with x_c, while attributing to $-C_{xx}x_c$, $-C_{xy}x_c$ those in quadrature with x_c. It can be shown that this leads to the definitions

$$K_{xx} = -\frac{F_d(\Omega) + F_d(-\Omega)}{2r} \qquad C_{xx} = -\frac{F_q(\Omega) - F_q(-\Omega)}{2\Omega r}$$

$$\tag{16}$$

$$K_{xy} = -\frac{F_q(\Omega) + F_q(-\Omega)}{2r} \qquad C_{xy} = -\frac{F_d(\Omega) - F_d(-\Omega)}{2\Omega r}$$

A geometrical interpretation of the difference between equations (15) and (16) is shown in fig. 3. Experimental or analytical determination of the set (16) of coefficients requires data on F_d and F_q at both Ω and $-\Omega$.

The K's and C's given by (15) and (16) coincide only if F_d and F_q are linear functions of Ω. Since either definition may be used in the literature with little elaboration, it would be of interest to study the extent to which this leads to numerical differences; pending this, we will in this study adopt the definitions (16). An example for a single-chamber seal is shown in Appendix 3. From this limited evidence, it appears that the important coefficients K_{xy}, C_{xx} are about the same in both definitions.

4. Comparison to Literature Data

4.1 Data Used

Benckert and Wachter have published an extensive set of data (refs. 11,16) for multichamber labyrinth seals of simple "straight" or "full" types (fig. 4). The data were taken in a static-offset rig operating on pressurized air, and induced forces were obtained by integration of measured azimuthal pressure variations on a number of seal cavities. Labyrinths with up to 23 chambers were used. The experiments allowed variation of shaft speed, ω, overall pressure ratio P_{atm}/P_o , rotor eccentricity r, seal geometry (δ_i , ℓ_i , h_i , Fig. 1), number of chambers and entry swirl c^* . The seal flow rate q was measured and an averaged carry-over factor μ was deduced from these data and reported in a number of instances. In our calculations we used these "measured" factors when available directly; in other cases, we adopted values measured for chambers of the same geometry, or, for the "full" type of seal, where little carryover is expected we used $\mu = 1$. The contraction coefficient c_c was taken as a function of Reynolds number and strip geometry as given by Vermes (ref. 17) (fig. 5).

Data of Brown and Leong (ref. 18) were also used for validation of the undisturbed flow predictions.

4.2 Undisturbed Flow Parameters

Figure 6 compares Brown and Leong's data on the axial pressure distribution in an 11-chamber test seal with our calculated undisturbed pressure distribution. There is good agreement except for the sharp pressure drop shown by the data between the inlet and the first chamber. This is probably a reflection of a reduced carry-over factor on the first strip; the calculation used a constant μ (the value used is irrelevant to the comparison).

Benckert and Wachter reported for one particular case the axial variation of azimuthal velocities c_i^* . This was for a 23-chamber seal with $c_o^* = 40$ m/sec, $P_a/P_o = .66$, $R_s = 0.15$ m, $\omega = 1000$ rad/sec, $r_1 = 0.25$ mm, $r_2 = 0$, $\delta^* = 0.5$ mm, $\ell_i = 4$ mm and $h_i = 6$ mm. The data are shown in figure 7, together with the code predictions. The good agreement shown is important for the prediction of disturbance side forces, which depend critically on swirl velocities. These results appear to validate the formulation used for the friction factors between the fluid and the stator and rotor surfaces (turbulent pipe flow formulae with a standard correction for "pipe" curvature).

4.3 Stiffness Coefficients Without Shaft Rotation

The cross-spring coefficients $K_{yx} = - K_{xy}$ for a number of cases from Benckert and Wachter's tests with a non-rotating shaft were calculated and the results are summarized in Table 2 and figure 8. The key in Table 2 describing the test parameters is explained in Table 1.

The eccentricity r_1 used in the tests was 0.15 mm, except for Run 17, which had $r_1 = 0.25$ mm.

Table 1. Key for Table 2 (2nd column)

	(Type, h, δ, ℓ)		
Type	h: chamber height	δ: clearance	ℓ: pitch
S = Straight-through	0 = 2.75 mm	0 = 0.25 mm	0 = 5 mm
F = Full-interlocking	1 = 6.25 mm	2 = 0.5 mm	1 = 8 mm
	3 = 6 mm		2 = 4 mm

As figure 8 illustrates, the calculated values are somewhat lower than the data (about 19% for series (s,0,0,0), 5% only for series (s,1,0,0)). The trends of the calculation are in agreement with those observed in the tests. In particular, K_{yx} is seen in figure 9 to be approximately proportional to inlet swirl and to overall pressure ratio, both in the tests and in the calculations (although, as mentioned, with a somewhat lower proportionality factor in the latter case).

4.4 Stiffness Coefficients with Shaft Rotation

Results similar to those in the previous section, but including various shaft speeds are given in Table 3 and figure 10. The eccentricity is still static (no whirl, $\Omega = 0$), and is 0.25 mm in all cases. The parameter E_0^* was used in Ref. 11 to correlate entry swirl, and is

$$E_0^* = \frac{\frac{1}{2}\rho_o\,(c_o^*)^2}{p_o + \frac{1}{2}\rho_o\,V_{ax,o}^2 - p_a} \; ; \; V_{ax,o} = \frac{q^*}{\rho_o \delta_1^*} \tag{17}$$

The comparison of data and theory shown in figure 10 indicates more scatter, but less systematic deviation than in the cases without shaft rotation (figures 8 and 9). The agreement is best for all the cases with 17 chambers (solid symbols in figure 10), which show an average error of 8.5% and little scatter.

4.5 Discussion

The two principal sources of uncertainty in our calculations are the friction factors (λ', λ'') and the carry-over coefficient β. The friction factor could in principle be substantially increased by the relative rotation of shaft and casing, since the fluid in each chamber is strongly sheared and develops marked secondary flow patterns, leading to enhanced mixing. Examination of data[19] for the somewhat related case of turbulent pipe flow with swirl does indeed show friction increases of up to a factor of four at high swirl. An accurate prediction of wall friction under the complex flow conditions of a labyrinth gland is not possible at this time, and this is an area requiring more experimental and analytical work.

The impact of friction factor inaccuracies on calculated cross-spring coefficients could be important, although not easily generalizable. In general, the cross-forces increase with the deviation between the swirl velocity and its frictional equilibrium value. An increase in wall friction in a non-rotating seal will accelerate the approach to this ultimate swirl, thus reducing the number of chambers where the excess or defect swirl is strong and thereby reducing the magnitude of K_{yx}

(whether positive or negative). This trend is always apparent at large enough friction coefficients, and especially for long multichamber seals. However, for short seals and weak frictional coupling a different effect dominates, namely the cross-stiffness tends to a limiting value independent of shaft rotation and in the direction of the inlet swirl. An example of this behavior for a one-chamber seal is presented in Appendix 3, figure A2, where it can be seen that for this particular case, increasing friction would lead to <u>increases</u> in $|K_{yx}|$. The behavior typical of long seals and large friction is illustrated in figure 11, corresponding to case 1 of Table 2; here, an increase of the friction factor above the nominal value leads to a <u>reduced</u> K_{yx}, although a reduction by more than about 0.6 would lead to the same effect.

The carry-over coefficient β is clearly another source of uncertainty in the model. The sensitivity of calculated cross-stiffness to β (or $\mu = \beta c_c$) is illustrated in figure 12, corresponding to parametric variations on Run 11 of Table 2, and figure 13 (from Run 7 of Table 3). The opposite trend in these two cases is due to the fact that in figure 12 the entry swirl is greater than its asymptotic value (reached after an infinite number of chambers), while the opposite is true in figure 13. In both cases, an increase of μ increases the flow rate q, which has the effect of delaying the transition towards the asymptotic c^*; in figure 12 this means higher c_i^* in the first 10-12 chambers, with correspondingly larger cross-forces; in figure 13, the same delaying effect at higher μ implies <u>lower</u> c_i^* values in the first 6-8 chambers, and, consequently, lower cross-forces.

Unfortunately, the state of the art in *a priori* predictions of β is not satisfactory. A fuller discussion of this point is given in reference 15. Basically, the best-known models (Vermes (ref. 17), Egli (ref. 20), Komotori (ref. 21)), indicate substantially different variations of the carry-over factor with number of chambers, with Vermes' model taking no account of this number at all. The best hope here lies with the numerical methods which are now beginning to be applied to internal flow problems in seals, although the somewhat primitive state of affairs with respect to calculations of fully separated turbulent flows still indicates a need for improvements. Thus Wadia and Booth (ref. 22) analyzed seal flows with no rotation and observed discrepancies of up to 13% in calculated flow coefficients when compared to data. For dynamics studies in seals, these 2-D or 3-D methods may, in any case, be too laborious; their proper role should probably be in furnishing improved semi-empirical results for integration into a simple multi-chamber lumped-parameter model, of the type considered here.

5. Parametric Studies

Reference 15 includes a variety of calculations that illustrate the trends of the force coefficients versus variations of seal parameters. Only some of the salient results will be mentioned here.

(a) K_{yx} increases linearly (but not proportionally) with entry swirl velocity. For conditions where the entry swirl exceeds the asymptotic azimuthal velocity, K_{yx} is generally positive, leading to excitation of forward whirl (with respect to the swirl direction). The reverse may be true at lower entry swirls. There is in some cases a value of entry swirl at which K_{yx} is zero.

(b) For multichamber seals with low entry swirl, the first few chambers contribute negative K_{yx} values, while those towards the end of the seal contribute positive values. Thus as the seal is made longer, the sign of K_{yx} may at some point

reverse. For seals where the entry swirl exceeds the ultimate azimuthal velocity, no such reversal occurs.

(c) The damping coefficient C_{xx}, which, together with K_{yx} controls the side force F_q, is positive in all cases studied, leading to stabilizing forces of the same order as those due to K_{yx}. This point will be more fully discussed in what follows.

6. Considerations on Fluid Damping

An example of calculated damping coefficients is shown in figure 14 (corresponding to the seal configuration of Run 1 in Table 3). A whirl (critical) frequency of 739 rad/sec was assumed; at the commonly found ratio $\omega/\Omega = 2$ for instability onset, $C_{xx} = 220$ N sec/m , giving $\Omega C_{xx} = 1.626 \times 10^5$ N/m. This is several times larger than K_{yx}, and indicates that seal damping forces are in this case sufficient to ensure stability. Another example of this behavior is shown by the single-cavity seal of Appendix 3; here $+ \Omega C_{xx}$ is roughly comparable to K_{yx} (but smaller).

A very simplified dynamic model will help to put in perspective the roles of the different coefficients in stability analysis. Assuming a shaft with mass M and structural stiffness K_o, the equations of motion for small side displacements x,y can be combined into

$$M \ddot{z} + \hat{C} \dot{z} + \hat{K} z = 0 \tag{18}$$

where $\hat{C} = C_{xx} + i C_{xy}$, $\hat{K} = K_o + K_{xx} + i K_{xy}$ and $z = x + iy$.

Assuming K_{xx}, K_{xy}, $C_{xx}^2/4M$ and $C_{xy}^2/4M$ are all small compared to K_o, as is likely to be the case in practice, we can define the (small) nondimensional parameters

$$k_{ij} = \frac{K_{ij}}{K_o} \quad ; \quad \zeta_{kj} = \frac{C_{ij}}{2\sqrt{K_o M}} \tag{19}$$

Then a simple analysis shows that, to the first approximation, the shaft complex displacement z will vary as $e^{\Omega_s t}$, where

$$\frac{\Omega_s}{\sqrt{K_o/M}} \simeq (- \zeta_{xx} \pm \frac{1}{2} k_{xy}) + i (\pm 1 \pm \frac{1}{2} k_{xx} - \zeta_{xy}). \tag{20}$$

Thus any nonzero k_{xy} will be destabilizing (in one or the other whirl direction), while a negative ζ_{xx} will be always destabilizing; k_{xx} and ζ_{xy} will simply modify the shaft natural frequency. Also, the effects of equal values of $|K_{xy}|$ and $- \Omega C_{xx}$ are seen to be equivalent.

This discussion has served to indicate that knowledge of the damping factor C_{xx} is at least as essential to studies of fluid-induced destabilizing forces as is the side force factor K_{xy}. Yet, due to the more difficult experimental conditions, much fewer data are available on C_{xx} than on K_{xy}.

We are now in the design stage of a test rig intended to address this problem. The general size and flow parameters will be similar to those used by Benckert and Wachter, but the sealed shaft will be made to execute forced whirling motion at speeds controlled separately from the spinning motion. Pressure distributions will be dynamically measured and integrated to produce values of the direct and transverse forces F_d, F_q for a range of whirl speeds Ω. Both K and C coefficients can then be extracted by the methods described in this paper. These features are similar to those of a rig described in reference 23 for tests in water.

7. Conclusions

A linear analytical model for the prediction of fluid forces in labyrinth seals has been presented and discussed. Comparison to literature test data shows reasonable agreement for the important cross-stiffness K_{yx}. The importance of the damping factor C_{xx} has been highlighted and the need for damping data made clear.

References

1. Ek, M.C., "Solution of Subsynchronous Whirl Problem in the High Pressure Hydrogen Turbomachinery of the Space Shuttle Main Engine." SAE 14th Joint Propulsion Conference, 78-1002, July 25-27, 1978.

2. Ehrich, F.F., "Identification and Avoidance of Instabilities and Self-Excited Vibrations in Rotating Machinery," ASME Paper 72-DE-21, Oct. 1979.

3. Ehrich, F.F. and Childs, D., to appear in the ASME Journal.

4. Wohlrab, R., "Experimental Determination of Gap Flow-Conditioned Forces at Turbine Stages and Their Effect on the Running Stability of Simple Rotors." NASA TM-77293, Oct. 1983 (Translated from Doctoral Thesis at the Muenchen Tech. Univ., 1975).

5. Urlichs, K., "Clearance Flow-Generated Transverse Forces at the Rotors of Turbomachines." NASA TM-77292, Oct. 1983. (Translated from Doctoral Thesis at the Muenchen Tech. Univ., 1975).

6. Pollman, E., Schwerdtfeger, H., Termuehlen, H., "Flow Excited Vibrations in High-Pressure Turbines (Steam Whirl)."

7. Alford, J.S., "Protecting Turbomachinery from Self-Excited Rotor Whirl." Journal of Engineering for Power, October 1965.

8. Kostyuk, A.G., "A Theoretical Analysis of the Aerodynamic Forces in the Labyrinth Glands of Turbomachines." Teploenergetica, 1972, 19 (11), pp 29-33.

9. Iwatsubo, T., "Evaluation of Instability Forces of Labyrinth Seals in Turbines or Compressors." NASA CP 2133, May 1980.

10. Childs, D.W., "Dynamic Analysis of Turbulent Annular Seals Based on Hirs' Lubrication Equation." ASME Tr., Journal of Lubrication Technology, Vol. 105, pp 429-436. Also, "Finite Length Solutions for Rotordynamic Coefficients of Turbulent Annular Seals." Ibid., pp 437-445.

11. Benckert, H. and Wachter, J., "Flow-Induced Spring Coefficients of Labyrinth Seals for Application in Rotor Dynamics." NASA CP 2133, May 1980.

12. Wright, D.V., "Air Model Tests of Labyrinth Seal Forces on a Whirling Rotor." _Journal of Engineering for Power_, Trans. ASME, Vol. 100, p 533, 1978.

13. Childs, D.W. and Dessman, J.B., "Testing of Turbulent Seals for Rotordynamic Coefficients." NASA CF 2250, pp 157-171, May 1982.

14. Celorio-Villaseñor, A., "Analysis of Disturbing Aerodynamic Forces in Labyrinth Seals." MS Thesis, Dept. of Aeronautics and Astronautics, MIT, September 1982.

15. Lee. O.W.K., "Prediction of Aerodynamic Force Coefficients in Labyrinth Seals." MS Thesis, Dept. of Aeronautics and Astronautics, MIT, February 1984.

16. Benckert, H., "Stromungsbedingte Fedeskennwerte in Labyrinthdichtungen." Doctoral Thesis, Univ. of Stuttgart, October 1980.

17. Vermes, G., "A Fluid-Mechanics Approach to the Labyrinth Seal Leakage Problem," _Journal of Basic Engineering_, Tr. ASME, Series D, Vol. 82, No. 2, June 1960, pp 265-275.

18. Leong, Y.M.M.S. and Brown, R.D., "Circumferential Press Use Distribution in a Model Labyrinth Seal, NASA CP 2250, May 1982.

19. Nissan, A.H. and Bresan, V.P., "Swirling Flow in Cylinders," A.I. _Ch. E. Journal_, Vol. 7, No. 4, Dec. 1961, pp 543-547.

20. Egli, A., "The Leakage of Steam Through Labyrinth Seals," Trans. ASME, Vol. 57, 1935, pp 115-122.

21. Komotori, K., "A Consideration on the Labyrinth Packing of Straight-Through Type Seals," _Nihon Kikai Gakkai_, Trans. J.S.M.E., Vol. 23, No. 133, 1957, pp 617-623.

22. Wadia, A.R. and Booth, T.C., "Rotor Tip Leakage: Part II - Design Optimization Through Viscous Analysis and Experiment." ASME Paper 81-GT-72.

23. Adams, M.L., Mackay, E., and Diaz-Tous, I.A., "Measurement of Interstage Fluid-Annulus Dynamical Properties." NASA CP 2250, pp 147-156, May 1982.

Appendix 1. The Unperturbed Solution

Squaring Eq. (1) and adding for all chambers yields for the nominal flow rate

$$q^* = \left[\frac{P_o^2 - P_a^2}{R_g T \sum_{i=1}^{K} \left(\frac{1}{\mu_i^2 \, \delta_i^{*2}} \right)} \right]^{1/2} \tag{A-1}$$

Also, adding for the first n chambers only gives

$$P_n^{*2} = P_o^{*2} - \frac{\sum\limits_{i=1}^{n} \left(\frac{1}{\mu_i^2 \delta_i^{*2}}\right)}{\sum\limits_{i=1}^{K} \left(\frac{1}{\mu_i^2 \delta_i^{*2}}\right)} (P_o^2 - P_a^2) \qquad (A-2)$$

The momentum equation (Eq. (3)) becomes in the steady state

$$q^*(c_i^* - c_{i-1}^*) + \tau_i' U' - \tau_i'' U'' = 0 \qquad (A-3)$$

with
$$\tau_i' = \frac{1}{8} \rho_i^* \lambda' c_i^{*2} \qquad (A-4)$$

$$\tau'' = \frac{1}{8} \rho_i^* \lambda'' (\omega R_s - c_i^*)^2 \qquad (A-5)$$

and λ (the Darcy friction factor) given by a modified pipe-flow expression

$$\lambda = \frac{0.3164}{R_e^{0.25}} [1 + 0.075 R_e^{0.25} \left(\frac{D_h}{2R_s}\right)^{1/2}] \times sign (v_{REL}) \qquad (A-6)$$

Here R_e is the Reynolds number based on chamber height and the corresponding relative flow velocity for fixed or rotating surfaces. The factor sign (v_{REL}) is needed to give the forces τ_i' , τ_i'' their proper direction. Thus, we append the factor sign (c_i^*) to λ' and the factor sign $(\omega R_s - c_i^*)$ to λ'' , both here and in the first order calculations of Appendix 2. D_h is the gland hydraulic diameter. Eqs. (A-3) through (A-6) can be solved for the distribution c_i^* of azimuthal velocities. In particular, the asymptotic velocity (c_∞^*) follows from (A-3) when $c_i^* = c_{i-1}^*$ is assumed.

Appendix 2. Coefficients for the Perturbation Equations

Let the transverse area of a gland (fig. 1) be $f_i^* = (h_i + \delta_i^*)\ell_i^*$ in the centered position. An asterisk on any variable denotes the undisturbed (centered) condition. We obtain for Eq. (7) the following coefficients.

$$A_i = \frac{f_i^*}{\gamma} \qquad B_i = \frac{c_i^* f_i^*}{R_s \gamma} \qquad C_i = \frac{c_i^* f_i^*}{R_s}$$

$$D_i = \frac{P_{i+1}^* \mu_i^2 \delta_{i+1}^{*2}}{P_i^* q^*} \qquad E_i = P_i^* \frac{\delta_{i+1}^{*2} \mu_{i+1}^2 + \delta_i^{*2} \mu_i^2}{q^*}$$

$$F_i = \frac{P_{i-1}^{*2} \mu_i^{*2} \delta_i^{*2}}{P_i^* q^*} \qquad\qquad J_i = \ell_i \qquad\qquad Z_i = \frac{c_i^* \ell_i}{R_s}$$

$$K_i = \frac{f_i^*}{\gamma} \qquad\qquad L_i = f_i^* \qquad M_i = \frac{f_i^*}{R_s}\left(\frac{c_i^*}{\gamma} + \frac{R_g T}{c_i^*}\right)$$

$$N_i = \frac{2c_i^* f_i^*}{R_s} \qquad\qquad O_i = \frac{P_{i+1}^{*2} \mu_{i+1}^2 \delta_{i+1}^{*2}}{P_i^* q^*}$$

$$P_i = \frac{P_i^* \mu_{i+1}^2 \delta_{i+1}^{*2}}{q^*} + \frac{P_i^* c_{i-1}^* \mu_i^2 \delta_i^{*2}}{c_i^* q^*} + \frac{U' \lambda' c_i^*}{8\,\gamma} - \frac{U'' \lambda''}{8 c_i^* \gamma}(\omega R_s - c_i^*)^2$$

$$Q_i = \frac{P_{i-1}^{*2} c_{i-1}^* \mu_i^2 \delta_i^{*2}}{P_i^* c_i^* q^*} \qquad\qquad R_i = \frac{q^*}{\rho_i^*} + \frac{\lambda' U'}{4} c_i^* + \frac{\lambda'' U''}{4}(\omega R_s - c_i^*)$$

$$S_i = \frac{c_{i-1}^*}{c_i^*}\,\frac{q^*}{\rho_i^*} \qquad\qquad W_i = \frac{q^*}{\rho_i^*}\left(\frac{1}{\delta_{i+1}^*} - \frac{c_{i-1}^*}{c_i^*}\frac{1}{\delta_i^*}\right)$$

$$X_i = \ell_i \qquad\qquad Y_i = \frac{c_i^* \ell_i}{R_s}$$

Here γ is the ratio of specific heats and R_g the gas constant.

Appendix 3. "Local" vs. "Global" Coefficients

Sample calculations were made for a single-chamber straight-through seal with $\delta = 0.25$ mm., $\ell = 8$ mm., $h = 3$ mm., $R_s = 15$ cm., $\omega = 1000$ rad/sec, $c_o = 100$ m/sec, $P_o = 1.5$ atm, $P_a = 1$ atm . For a range of whirl frequencies from $\Omega \cong 0$ to $\Omega = 750$ rad/sec, the resulting direct and quadrature forces are shown in figure Al. The quadrature force F_q , which is the one of importance for stability considerations, is seen to be very nearly linear with Ω, indicating no difference between the local and the global definitions of the coefficients (Eqs. (15) and (16), respectively).

There is, on the other hand, a slight curvature in the F_d line. The values calculated for $\Omega = 500$ rad/sec are as follows:

	K_{xx}(N/m)	K_{yx}(N/m)	C_{xx}(N sec/m)	C_{yx}(N sec/m)
Local (Eqs. (15))	610	11350	+ 13.7	- 0.95
Global (Eqs. (16))	652	11480	13.98	- 1.02

For the same seal, with $\Omega = 0$ throughout, figure A2 shows the effect of parametric variations of the friction coefficients (λ' and λ'' varied simultaneously) at various shaft rotation speeds.

Table 2. K_{yx} Calculated vs. Experimental ($\omega_{rot} = 0$)

						K_{yx}	
				C_{*_o}		Exper.	Calcula.
Run #	Seal Type	K	P_a/P_o	(m/s)	μ	(x 10^5 N/m)	
1	S,0,0,0	17	.66	38.4	.92	.75	.611
2	S,0,0,0	17	.32	52.9	.92	2.57	2.091
3	S,1,0,0	17	.32	68.3	1.02	1.57	1.45
4	S,1,0,0	17	.66	33.4	1.02	.27	0.274
5	S,1,0,0	17	.66	48.5	1.02	.423	0.411
6	S,1,0,0	17	.56	39.0	1.02	.457	0.410
7	S,1,0,0	17	.79	38.2	1.02	.218	0.224
8	S,0,0,0	17	.49	63.5	.92	1.89	1.586
9	S,0,0,0	17	.39	54.3	.92	2.22	1.747
10	S,0,0,0	17	.79	15.6	.92	.184	0.160
11	S,0,0,0	17	.49	64.2	.92	1.75	1.605
12	S,0,0,0	17	.49	34.5	.92	1.05	0.807
13	S,1,0,0	17	.49	82.68	1.02	.98	1.098
14	S,1,0,0	17	.49	40.78	1.02	.57	0.509
15	S,0,0,0	17	.32	38.2	.92	1.9	1.431
16	S,0,0,0	17	.32	27.6	.92	1.2	0.937
17	F,3,2,1	9	.49	144.7	.665	1.47	1.606
18	S,0,0,0	17	.32	45.5	.92	2.39	1.757

Average error (in absolute value) = 18.3%

(4.5% for (S,1,0,0) , 18.6% for (S,0,0,0)).

Table 3. K_{yx} Calculated vs. Experimental ($\omega_{rot} \neq 0$)

							K_{yx}	
				C_{*_o}	ω_{rot}		Exper.	Calcula.
Run #	Seal Type	K	P_a/P_o	(m/s)	(rad/s)	μ	(x 10^5 N/m)	
1	F,3,2,2	17	.66	43.2	1000	.66	.189	0.177
2	F,3,2,2	23	.66	47.1	1000	.66	.44	0.349
3	F,3,2,2	23	.66	40.	1000	.66	.38	0.315
4	F,3,2,2	23	.79	---	993.3	.66	.307	---
5	F,3,2,2	23	.793	66.2	993.3	.66	.323	0.398
6	F,3,2,2	23	.793	49.8	746.67	.66	.189	0.228
7	F,3,2,2	17	.793	50.7	993.3	.66	.248	0.230
8	F,3,2,2	23	.657	86.74	993.3	.553[1]	.442	0.398
9	F,3,2,2	23	.657	83.64	746.67	.606[1]	.290	0.340
10	F,3,2,2	17	.66	27.9	1000	.66	.112	0.088
11[2]	F,3,2,2	17	.66	43.2	1000	.66	.20	0.187
12[2]	F,3,2,2	17	.66	27.9	746.67	.66	.12	0.0849
13[2]	F,3,2,2	17	.66	15.5	500.	.66	.044	0.0178
14[3]	F,3,2,2	23	.66	47.1	1000	.66	.40	0.328
15[3]	F,3,2,2	23	.66	30.	746.67	.66	.23	0.170
16[3]	F,3,2,2	23	.66	54.7	500	.66	.09	0.123

1 -- μ calculated from measured mass flow rate: friction factor for a
    channel used.
2 -- resultant forces from chambers 7 - 17 only.
3 -- resultant forces from chambers 7 - 23 only.
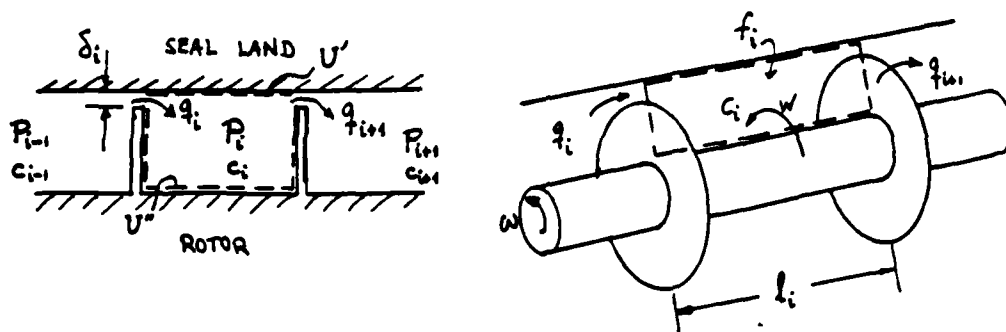
Average error (in absolute value) = 23.0%
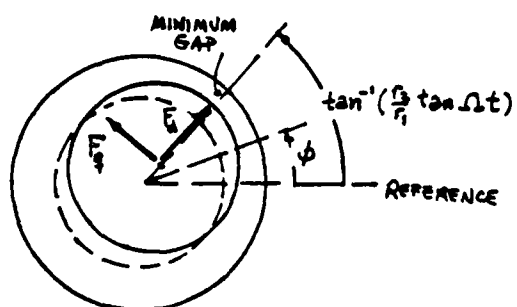
Fig. 1 Geometry for labyrinth seal analysis

Fig. 2 Direct (F_p) and quadrature (F_q) forces
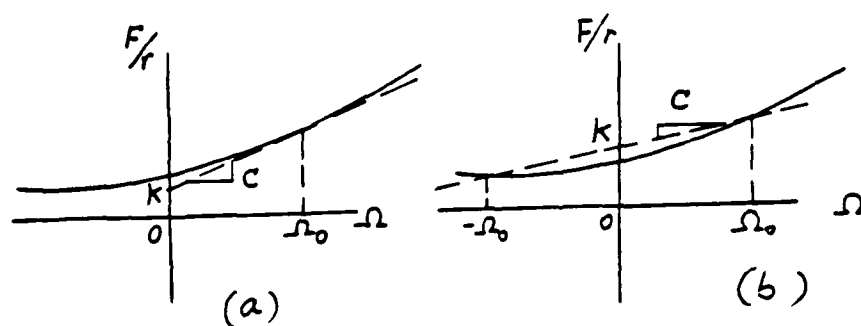due to rotor eccentricity

Fig. 3 Two different definitions of spring and
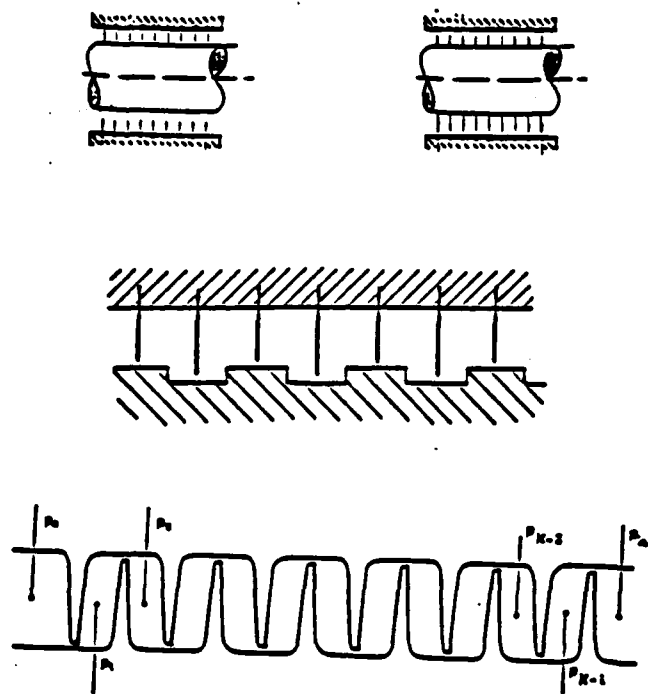damping coefficients.
(a) Local (Eqs.15), (b) Global (Eqs.16))

Fig. 4 Straight-through Stepped
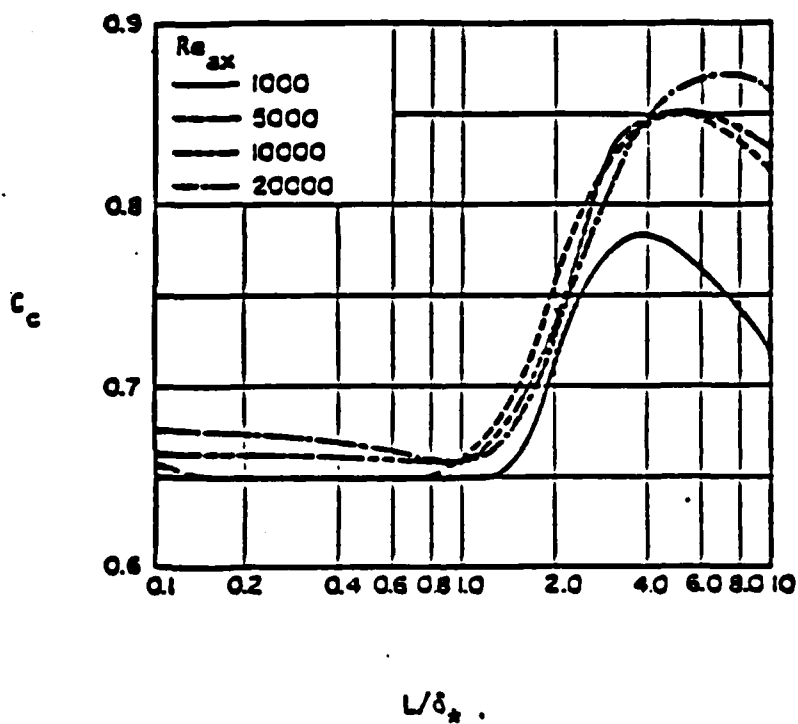and Full Labyrinth Seals
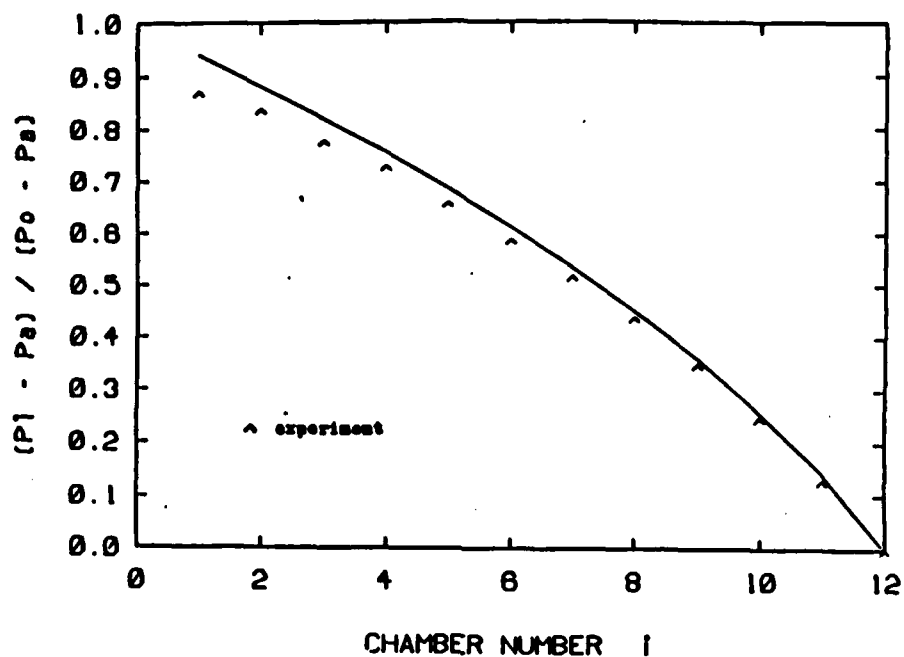

C_c

L/δ_* .

Fig. 5 Coefficient of contraction, C_c

Fig. 6   Calculated vs. experimental axial pressure distribution.
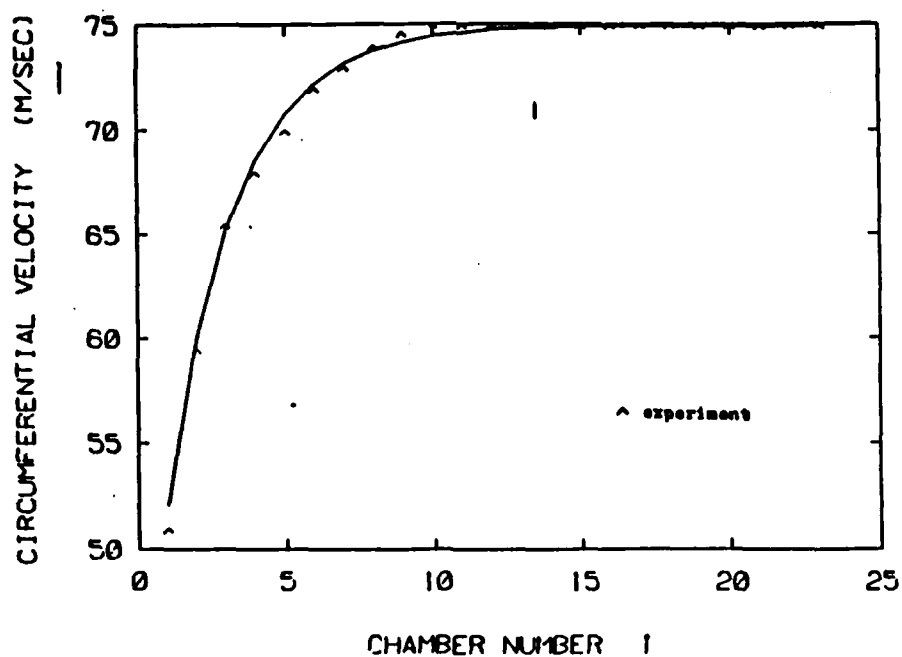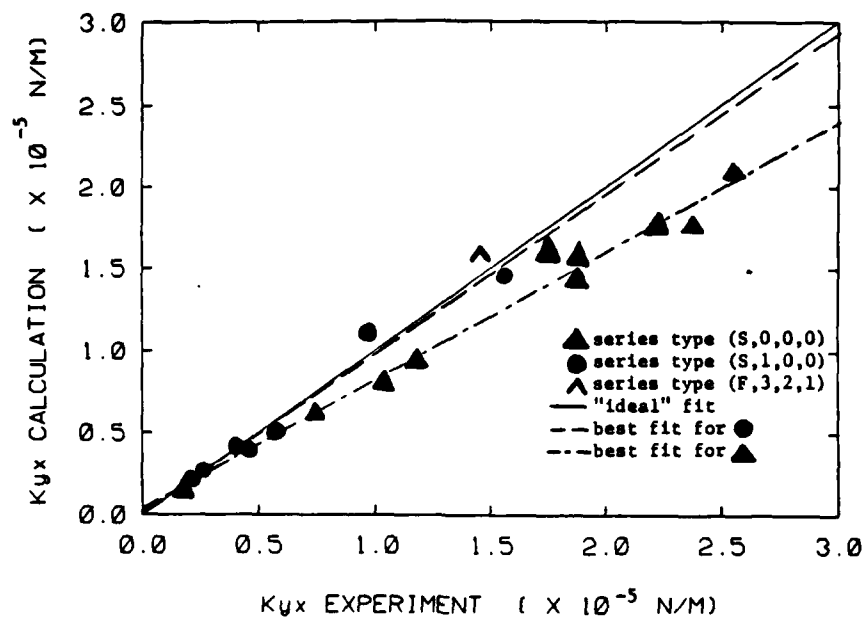

Fig. 7   Calculated vs. experimental circumferential velocity distribution

Fig. 8. Calculated vs. experimental cross spring coefficient Kyx (ω_{rot} = 0)
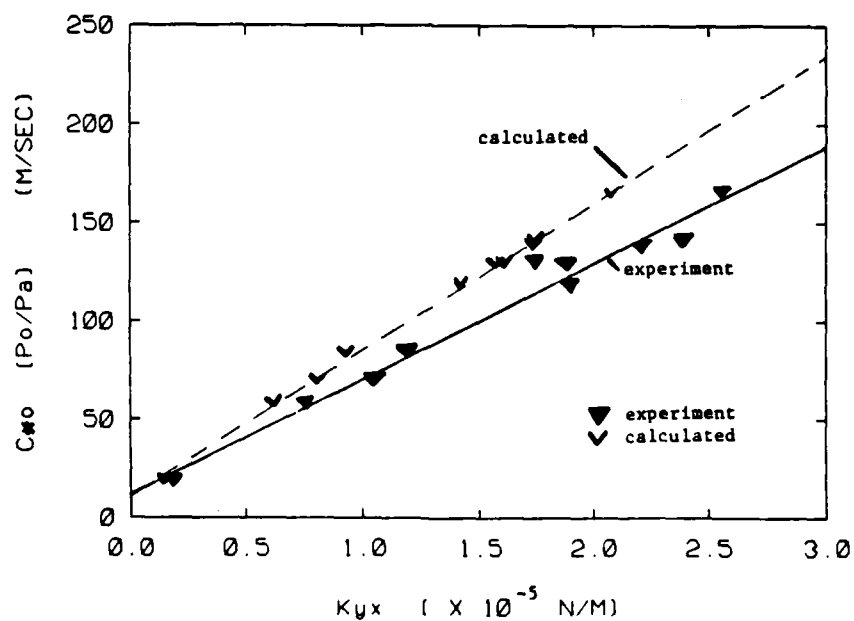
Fig. 9. Entry swirl parameter and calculated and experimental cross spring coefficient Kyx.
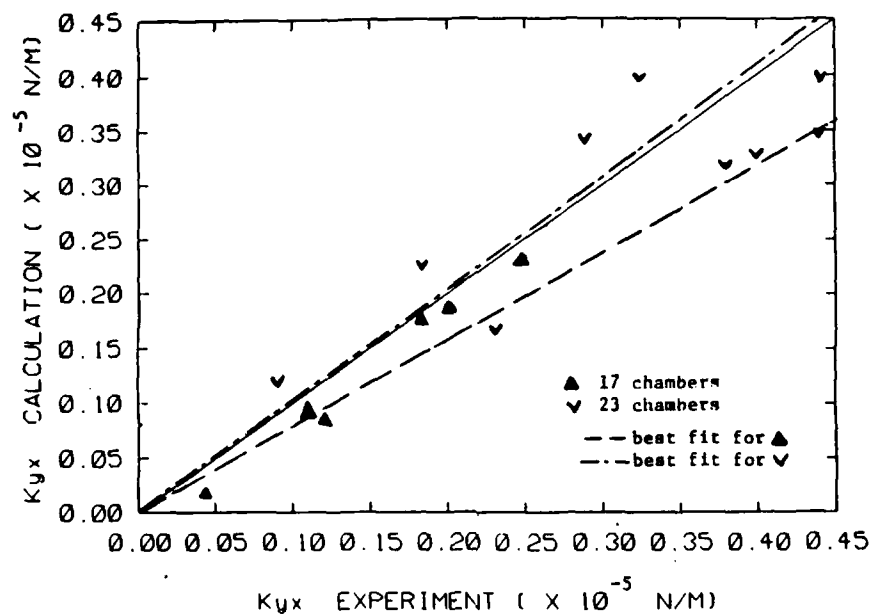
Fig. 10. Calculated vs. experimental cross spring coefficient Kyx ($\omega_{rot} \neq 0$)
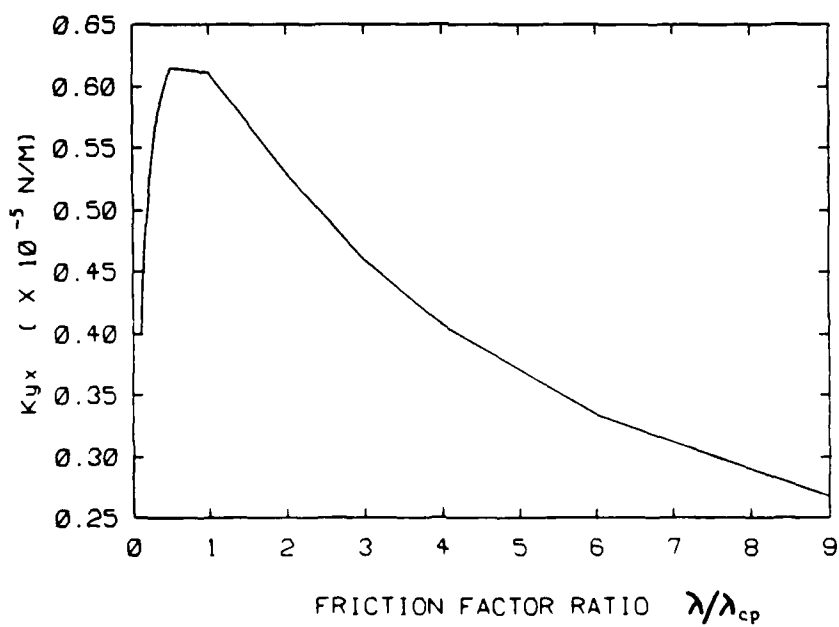
Fig. 11. Effect of friction factor on cross spring coefficient Kyx.
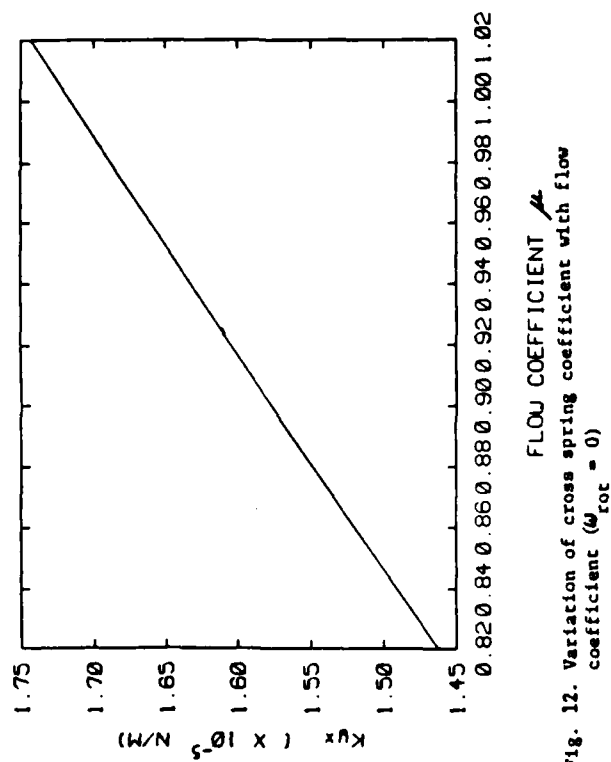
Fig. 12. Variation of cross spring coefficient with flow coefficient ($\omega_{rot} = 0$)
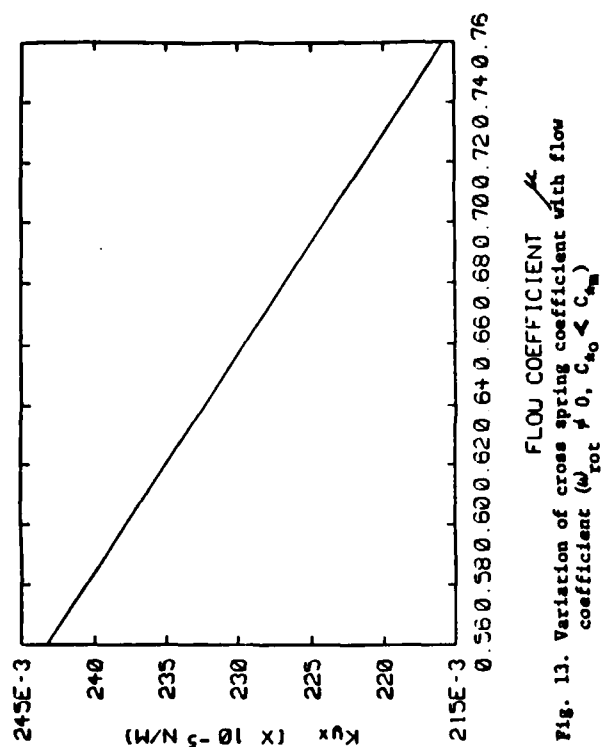
Fig. 13. Variation of cross spring coefficient with flow coefficient ($\omega_{rot} \neq 0$, $C_{R_0} < C_{R_m}$)

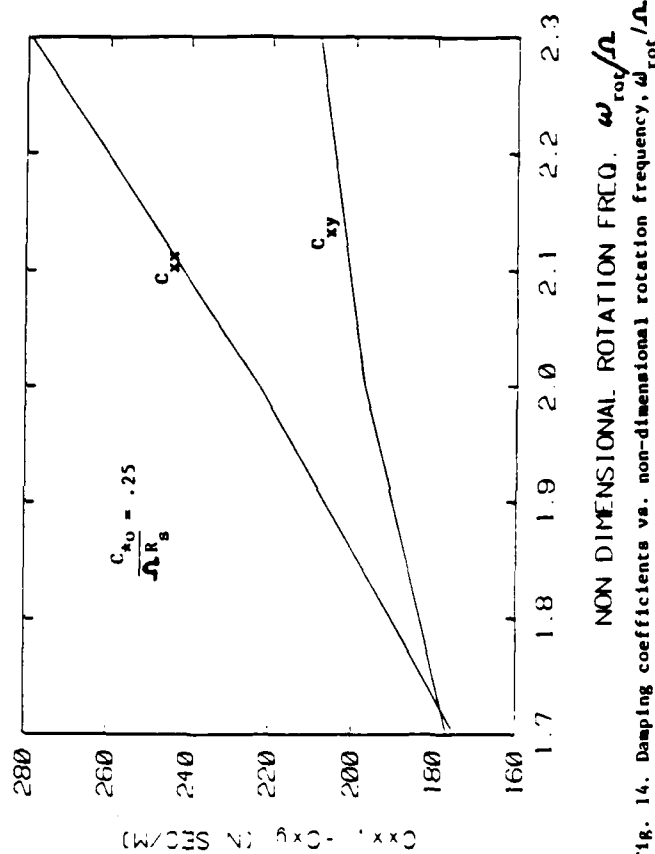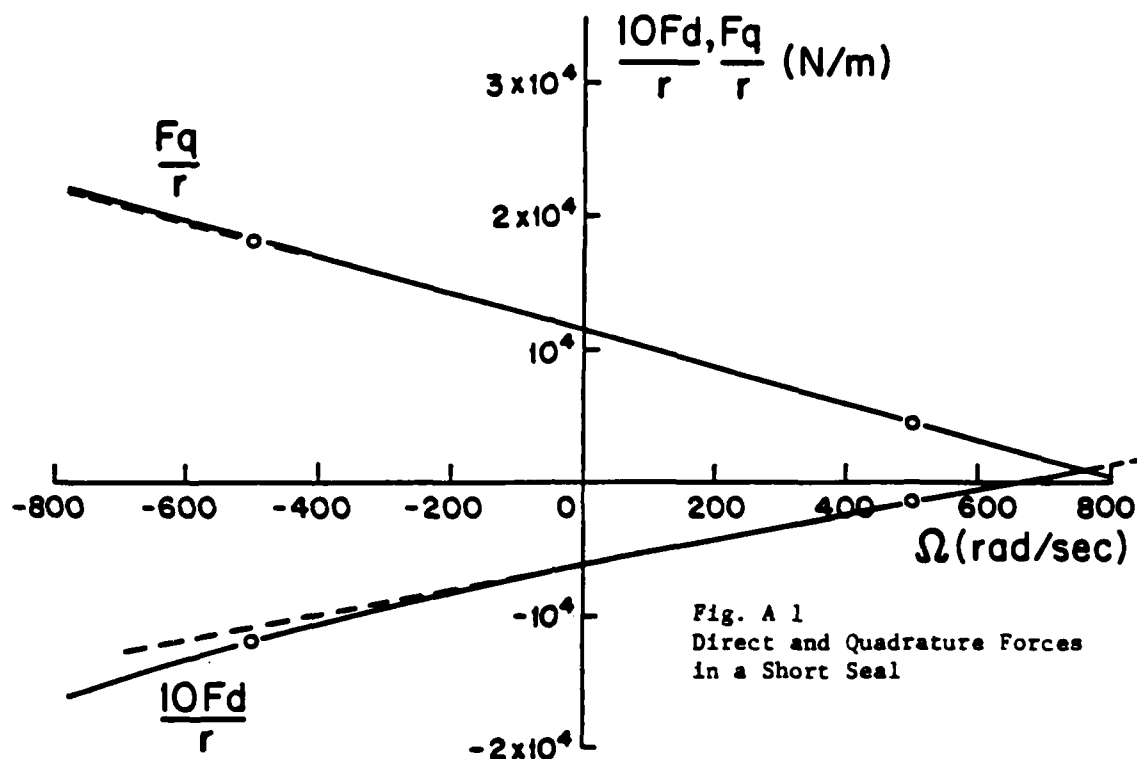Fig. 14. Damping coefficients vs. non-dimensional rotation frequency, ω_{rot}/Ω

Fig. A 1
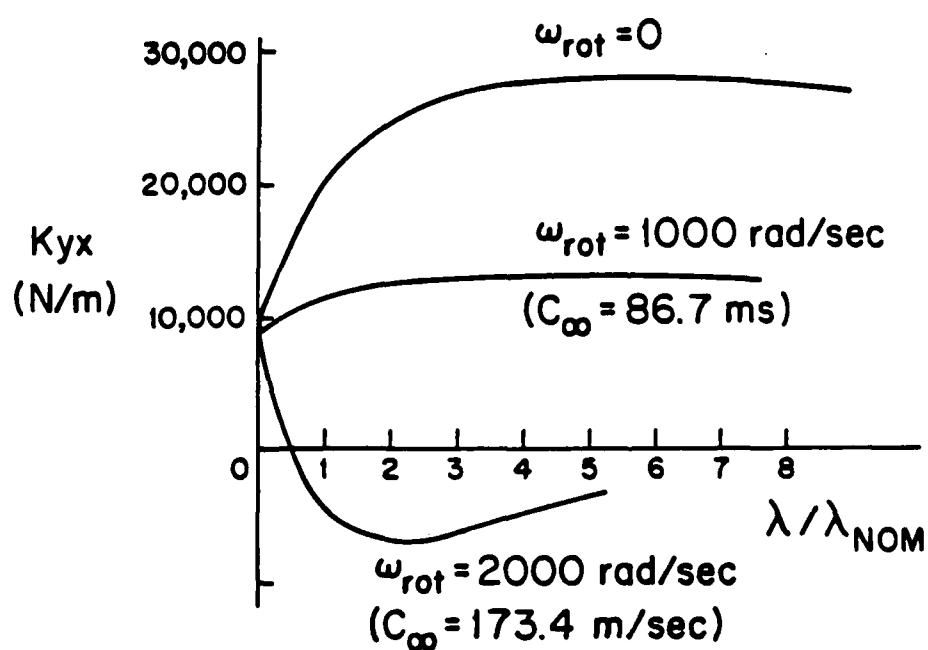Direct and Quadrature Forces
in a Short Seal

Fig. A 2   Effect of Friction Factor Variation
on Cross-Stiffness in a Short Seal.
Inlet Swirl Velocity C_o = 100 m/sec.

END

12-86

DTIC